

The Impact of Ink-Jet Droplets on a Paper-Like Structure

M. Do-Quang¹ A. Carlson¹ and G. Amberg¹

Abstract: Inkjet technology has been recognized as one of the most successful and promising micro-system technologies. The wide application areas of printer heads and the increasing demand of high quality prints are making ink consumption and print see-through important topics in the inkjet technology. In the present study we investigate numerically the impact of ink droplets onto a porous material that mimics the paper structure. The mathematical framework is based on a free energy formulation, coupling the Cahn-Hilliard and Navier Stokes equations, for the modelling of the two-phase flow. The case studied here consists of a multiphase flow of air-liquid along with the interaction between a solid structure and an interface. In order to characterize the multiphase flow characteristics, we investigate the effects of surface tension and surface wettability on the penetration depth and spreading into the paper-like structure.

Keywords: Multiphase flow, wetting surface, droplet impact, Cahn-Hilliard.

1 Introduction

Ink-jet technology has been recognized as one of the most successful and promising micro-system technologies. The wide application areas of print heads and the increasing demand of high quality prints are making ink consumption and print see-through important topics in the inkjet technology. In order to advance to a cheaper production of high quality prints, fundamental issues about the physics concerning the impact of ink droplets on paper structures needs to be resolved.

Many phenomena with a complex physics takes place from a droplet are ejected from the print head, until it has obtained its equilibrium form in the paper structure. In the first stage the droplet shoots out of the print head with a velocity typically ranging between $1 - 20 \text{ m} \cdot \text{s}^{-1}$ and it will often, as it travels towards the paper, form a tail that consist of small satellite droplets (Do-Quang, Geyl, Stemme,

¹ Linné Flow Centre, Department of Mechanical, Royal Institute of Technology, Stockholm, 100 44 SWEDEN. Email: minh@mech.kth.se

van der Wijngaart, and Amberg (2010)). It impacts the paper, which has a heterogeneous surface of cellulose fibers. These fibers are chemically treated, often with different degrees of wettability. After the droplet has impacted onto the surface it can either penetrate or recoil, depending on the papers roughness and wettability. Experiments by Kannangara, Zhang, and Shen (2006) showed that the forced spreading and droplet recoil after impact on commercial paper surfaces depended on their wettability. The surfaces were found to inherit a dual nature, and behaved as hydrophobic upon first contact with the impacting droplet allowing no ink to penetrate. Thereafter, during the droplet recoil process it behaved like a hydrophilic surface. If the droplet fully recoils or if it is sufficiently large it can make a splash so that the ink spreads over a larger part of the paper, thus reducing the prints quality. How to trigger the splash of a droplet has been a matter of intense investigation in the literature (Yarin (2006)), where the wettability, surface structure (Xu, Barcos, and Nagel (2007)) and environmental pressure (Xu, Zhang, and Nagel (2005)) have all been identified as key parameters to trigger or suppress splashing.

After the droplet has impacted onto the paper, wetting will dominate the droplet infiltration into the paper structure. Since the surface often has a heterogeneous structure, consisting of fibers with different wetting properties, that also adsorbs the liquid poses additional challenges to the already complex wetting physics that one observed on relatively smooth solid surfaces see Blake (2006); Bonn, Eggers, Indekeu, Meunier, and Rolley (2009). Modaressi and Garnier (2002) found in experiments that the droplet evolve into the paper as a function of two sequential phenomena. First, the droplet spreads into the material, forming its footprint in the paper, until it reaches its pseudo-equilibrium contact angle. After the droplet has reached its pseudo-equilibrium state it starts to adsorb into the bulk of the paper material.

Numerical simulations of the impact of a droplet on a porous surface were performed by Alam, Toivakka, Backfolk, and Sirvio (2007) with the Volume of Fluid method, Hyvaluoma, Raiskinmaki, Jasberg, Koponen, Kataja, and Timonen (2006) with the Lattice Boltzmann method and by Reis, Griffiths, and Santos (2004) with a marker-cell method. These have both in common that the droplet size was much larger than the characteristic roughness of the porous media. Alam, Toivakka, Backfolk, and Sirvio (2007) examined the effect of surface structures and found that a sustained pressure outside the porous media increased the adsorption depth as a function of time.

Here, we adopt the Phase Field method to numerically investigate the impact of an ink-droplet onto a paper-like structure. The case studied here consists of a mul-

tiphase flow of air-liquid along with the interaction between a solid structure and an interface. We focus on the initial regime, before adsorption of the liquid into the bulk surface material, and seek to characterize the pseudo-equilibrium regime as reported by Modaressi and Garnier (2002). A small droplet with the same size as the characteristic surface roughness is considered as it impacts a web of cellulose fibers, mimicking the paper structure. By only changing the fibers wettability we show that the droplet can either penetrate or bounce as it impacts the paper-like structure.

1.1 Governing equations

Several authors have previously demonstrated the applicability for the diffuse interface method to describe two-phase flows (Anderson, McFadden, and Wheeler (1998); Jacqmin (1999)). Do-Quang and Amberg (2009) and Do-Quang, Geyl, Stemme, van der Wijngaart, and Amberg (2010) has demonstrated the capability of this method for the simulations of liquid-gas systems. Here, we will briefly describe the main ideas and list the governing equations, for a mixture of two Newtonian fluids.

In the phase-field model, the order parameter or phase-field ϕ , is has a distinct equilibrium value representing the two phases, but it changes rapidly but in a smooth fashion between the two equilibrium states across the interface. Here takes the value $\phi = 1$ in liquid phase and $\phi = -1$ in gas phase. The free energy of the system is described by a Ginzburg-Landau expansion of the free energy of the system (Cahn and Hilliard (1958)),

$$\mathcal{F} = \int_{\Omega} \left(\beta \psi(\phi) + \frac{\alpha}{2} (\nabla \phi)^2 \right) d\Omega + \int_{\Gamma} g(\phi, \sigma) d\Gamma, \quad (1)$$

where α and β are constants that are related to the surface tension and interface thickness. $\psi(\phi)$ represents here the bulk energy and takes the form of a double-well potential function, with two minima $\phi = \pm 1$ corresponding to the two stable phases. ψ is here represented by,

$$\psi = \frac{1}{4}(\phi + 1)^2(\phi - 1)^2. \quad (2)$$

The second term in equation (1) describes the interface energy. This term associates with variations of the phase field ϕ and contributes the free-energy of the interfacial region, which defines the surface tension coefficient,

$$\sigma = \alpha \int_{-\infty}^{+\infty} \left(\frac{d\phi_0}{dx} \right)^2 dx = \frac{2\sqrt{2}}{3} \sqrt{\alpha\beta} \quad (3)$$

The free energy at the solid surface $d\Gamma$ is formulated by the surface energy contribution from the three interfaces appearing; solid (s), gas (g) and liquid (l), and $g(\phi, \sigma)$ is a function varying smoothly between the surface energies σ_{sl} and σ_{sg} (Jacqmin (1999)).

By taking the variational derivative of the free energy, \mathcal{F} , with respect to the order parameter ϕ and perform some algebra transformations, we obtain the Cahn and Hilliard (1958) equation,

$$\frac{\partial \phi}{\partial t} + (\mathbf{u} \cdot \nabla) \phi = \nabla \cdot (\kappa \nabla (\beta \Psi'(\phi) - \alpha \nabla^2 \phi)). \quad (4)$$

In this equation, the interface is not captured by a sharp interface. It uses, ϕ , a finite thickness, smooth transition region to distinguish the different phases. Here, κ is the constant mobility and η is the chemical potential, defined as

$$\eta = \beta \frac{\partial \Psi}{\partial \phi} - \alpha \nabla^2 \phi. \quad (5)$$

Once the phase field is calculated, the physical properties such as the density and the viscosity are calculated as follows,

$$\rho = \rho_l \frac{1 + \phi}{2} + \rho_g \frac{1 - \phi}{2}, \quad (6)$$

$$\mu = \mu_l \frac{1 + \phi}{2} + \mu_g \frac{1 - \phi}{2}, \quad (7)$$

where ρ_l, ρ_g and μ_l, μ_g are the densities and viscosities of the liquid and gas phase, respectively.

The fluid flow is described by the Navier-Stokes equations for an incompressible flow.

$$\rho \left(\frac{\partial \mathbf{u}}{\partial t} + \mathbf{u} \cdot (\nabla \mathbf{u}) \right) = -\nabla p + \nabla \cdot (\mu (\nabla \mathbf{u} + \nabla^T \mathbf{u})) + \eta \nabla \phi, \quad (8)$$

$$\nabla \cdot \mathbf{u} = 0, \quad (9)$$

where ρ denotes the density, \mathbf{u} the velocity vector, μ the viscosity, and p the pressure. The last term in equation (8) is expressing the potential form of the surface tension force, proposed by Jacqmin (1999).

1.2 Boundary conditions

In phase field theory, the wetting boundary condition for the interface is set via the balance of the free energy distribution between the different phases. By making

the assumption that the interface is at local equilibrium as it wets the surface, the boundary condition becomes Villanueva and Amberg (2006),

$$\alpha \nabla \phi \cdot \mathbf{n} + \sigma \cos(\theta_e) g'(\phi) = 0, \tag{10}$$

where θ_e is the static equilibrium contact angle. Here the contact angle is related to the surface tension coefficients σ through the Young's equation: $\sigma \cos(\theta_e) = \sigma_{lg} - \sigma_{sl}$. In Eq.(10), $g(\phi)$ is a normalized function varying smoothly from 0 to 1. It is used to localize the surface energy of each phases on the energy system. In our simulation $g(\phi) = 0.5 - 0.75\phi + 0.25\phi^3$.

The assumption of local equilibrium at the solid surface has been a widespread assumption in phase field wetting simulations, which has proven to be successful in describing numerous physical phenomena involving moving contact lines (Jacqmin (1999); Villanueva and Amberg (2006); Do-Quang and Amberg (2009); Do-Quang, Geyl, Stemme, van der Wijngaart, and Amberg (2010)). Recently, Carlson, Do-Quang, and Amberg (2009) has included the dissipative mechanism into the boundary condition of the Phase Field framework. It allows for the non-equilibrium wetting contact angle in rapid wetting. Such dissipative effects are assumed to be negligible here, thus applying the assumption of local equilibrium (Villanueva and Amberg (2006); Do-Quang and Amberg (2009)) as the liquid wets the solid surface using the boundary condition given in eq.(10).

1.3 Non-dimensionalization

The governing equations are made dimensionless based on the characteristic parameters of the flow, giving the dimensionless variables,

$$x' = \frac{x}{L_c}, u' = \frac{u}{U_c}, t' = \frac{tU_c}{L_c}, p' = \frac{p}{\rho_c U_c^2}, \tag{11}$$

where L_c is the characteristic length taken to be the droplet radius, U_c is the characteristic velocity taken to be the initial velocity of the ink droplet. ρ_c is the characteristic density defined as the water density. Dropping the primes, the dimensionless equations are

$$\rho(\phi) \frac{D\mathbf{u}}{Dt} = -\nabla p + \frac{1}{Re} \nabla \cdot (\mu(\phi)(\nabla \mathbf{u} + \nabla^T \mathbf{u})) + \frac{1}{Ca \cdot Cn \cdot Re} \eta \nabla \phi, \tag{12}$$

$$\nabla \cdot \mathbf{u} = 0, \tag{13}$$

$$\frac{D\phi}{Dt} = \frac{1}{Pe} \nabla \cdot (\kappa \nabla \eta), \tag{14}$$

$$\eta = \frac{\partial \Psi}{\partial \phi} - Cn^2 \nabla^2 \phi. \tag{15}$$

Note that incompressibility does not imply that the density is constant, only that the density is independent of pressure, which is a good approximation whenever flow speeds are small compared to speeds of sound. Also, note that the Peclet number in eq.(14) is large, due to the small value of the diffusion coefficient. Eq.(14) then essentially states that ϕ , and thus density, is constant along a streamline, which is consistent with the assumption of incompressibility in eq.(13).

The dimensionless parameters are the Capillary number Ca , Reynolds number Re and Peclet number Pe and Cahn number Cn ,

$$Pe = \frac{U_c L_c}{D}, Cn = \frac{\xi}{L_c}, Re = \frac{\rho_c U_c L_c}{\mu}, Ca = \frac{\mu_c U_c}{\sigma}, \quad (16)$$

where μ_c is the characteristic viscosity taken to be the liquid ink viscosity, D is the diffusivity of liquid vapour in air, $\xi = \sqrt{\alpha/\beta}$ is the interface thickness. The Peclet (Pe) number expresses the ratio between advection and diffusion. The Cahn (Cn) number expresses the ratio between the interface width and the characteristic length scale. The Reynolds (Re) number expresses the ratio between the inertia and the viscous force. The Capillary (Ca) number expresses the ratio between the viscous and the surface tension force.

2 Numerical treatment

The numerical simulations were carried out using femLego (Amberg, Tönhardt, and Winkler, 1999), a symbolic tool to solve partial differential equations with adaptive finite element methods. The partial differential equations, boundary condition, initial conditions, and the method of solving each equation are all specified in a Maple worksheet. The Cahn-Hilliard equation is treated as a coupled system for the chemical potential η and the composition ϕ . Both the chemical potential and the composition equations are discretised in space using piecewise linear functions and discretised in time using an implicit scheme. The coupled nonlinear algebraic system of η and ϕ is solved by an exact Newton's method. Within each Newton iteration, the sparse linear system is solved by unsymmetric multifrontal method UMFPACK, Davis (2004).

To ensure mesh resolution along the vicinity of the interface, an adaptively refined and de-refined mesh is used with an ad-hoc error criterion function,

$$\varepsilon \int_{\Omega_k} \nabla^2 \phi \leq \text{tol}. \quad (17)$$

The implementation of the mesh adaptivity can be described as follows. At each mesh refinement step, an element Ω_k is marked for refinement if the element size is still larger than the minimum mesh size allowed, $h > h_{min}$, and it does not meet

the error criterion (17). ε is an ad hoc parameter. In the case that an element meets the error criterion, it is marked for de-refinement unless it is an original element. At the next refinement step, elements containing hanging nodes are marked for refinement. The refinement/de-refinement stops if and only if no element is marked for refinement/de-refinement. More details about this scheme can be found in Villanueva and Amberg (2006); Do-Quang, Villanueva, Singer-Loginova, and Amberg (2007); Do-Quang and Amberg (2009).

The Navier-Stokes equations are solved using a projection method for variable density that was introduced by Guermond and Quartapelle (2000). The Navier-Stokes equations are also discretized in space using piecewise linear functions with the convective term treated as a semi-implicit term which allows a longer time step in the computations. The linear system is solved by the generalized minimal residual method (GMRES).

3 Numerical results and discussion

The performance and convergence of the method was tested on different problems where the motion was driven by surface tension. The gravitational forces are supposed to be small in our future applications. The gravity was therefore set to zero in all the computations presented here.

3.1 The Laplace law

Table 1: Deviation between the numerical and analytical pressure for different Cn numbers and mesh resolutions. Δx is the mesh spacing and P_{error} is defined as the relative error between the analytically and the numerically predicted pressure jump, $P_{error} = 100 \cdot \left(1 - \frac{(\Delta P)_{numerical}}{(\Delta P)_{analytical}}\right)$.

Cn	0.015	0.04	0.04	0.06	0.08
Δx	0.003	0.013	0.02	0.02	0.027
P_{error}	0.06%	0.6%	2.0%	0.6%	0.9%

We have measured the pressure jump for different mesh spacing and Cn numbers. The Cn number gives the ratio between the width of the diffuse interface and the characteristic length scale in the flow, here being the droplet diameter d . The results are summarized in table(1), where we have kept the $Ca = 1$, $Pe = 3 \cdot 10^{-3}$ and $Re = 1$ fixed. These dimensionless numbers gives an analytical pressure difference $(\Delta P)_{analytical} = 8\sqrt{2}/3$. The numerical domain has an extension of $[2d \times 2d \times 2d]$

and an equidistant mesh has been applied. Table(1) is summarizing the relative error between the computed and analytical pressure prediction for different Cn numbers and mesh spacings, after eight time steps. It is noted that the correct pressure is immediately obtained with good agreement between the numerical and analytical solution. One trend in table(1) is that the error in pressure depends on the numerical resolution of the interface. Another observation is that the correct pressure jump is obtained even with wide interfaces.

3.2 Droplet oscillations

The dynamic behavior of the surface tension model has been verified by validating the numerical simulations against an analytical expression for droplet oscillations in the absent of gravity. The droplet has a density ρ_1 and viscosity μ_1 submerged in an external fluid with a density ρ_2 and viscosity μ_2 . In cylindrical coordinates the droplet radius is given by

$$r = R_0(1 - \xi/4 + \xi P_n(\cos\theta)) \quad (18)$$

where R_0 is the initial droplet radius, P_n is the Legendre polynomial of order n , and $\xi \ll 1$. Fyfe, Oran, and Fritts (1988) extended the linear Rayleigh's theory for small amplitude oscillations on cylindrical jets and introduce an analytical expression for infinitesimal amplitude oscillations of an incompressible, inviscid droplet. The frequency ω for the droplet oscillation is given by

$$\omega = \sqrt{\frac{n^3 - n}{\rho_1 + \rho_2} \frac{\sigma}{R_0}}. \quad (19)$$

Several simulation were performed with different density ratios, where the non-dimension parameters have been kept constant as; $Re = 200$, $Ca = 0.01$, $R_0 = 1$, $n = 2$, $\xi = 0.01$. The evolution of the radius in time is shown in fig. 1. Table 2 shows the analytical result for the oscillation frequency (eq.(19)), numerical solution and their relative error for different density ratios.

Table 2: The analytical and numerical oscillation frequency (ω) and their relative error for different density ratios ρ_1/ρ_2 .

ρ_1/ρ_2	Analytical ω	Numerical ω	Error %
1	1.1892	1.1758	1.13
0.1	1.6035	1.5921	0.71
0.01	1.6734	1.6644	0.54
0.001	1.6810	1.6790	0.12

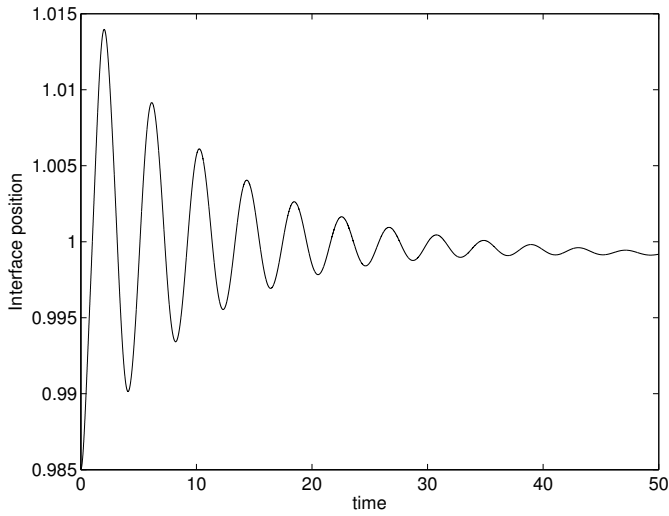


Figure 1: Evolution of the droplet radius.

It should be noted that the conservation of mass $m = \int_{\Omega} \rho dV$ is recorded in time, with only a $6.339 \times 10^{-6} \%$ mass variation from the initial to the final time.

3.3 The impact of the ink-jet droplets

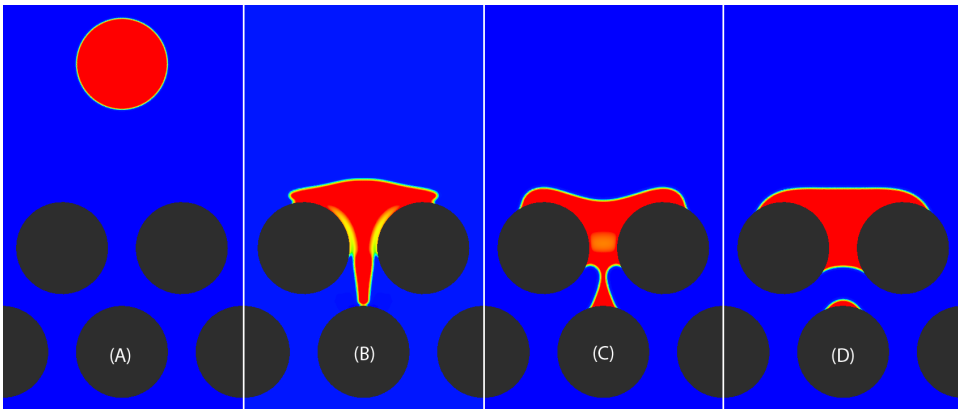


Figure 2: Impact droplet on a paper-like structure with the wetting contact angle $\theta = 30^\circ$. (A) at time reference $t = 0 \mu s$, (B) $t = 17 \mu s$, (C) $t = 34 \mu s$ and (D) $t = 85 \mu s$

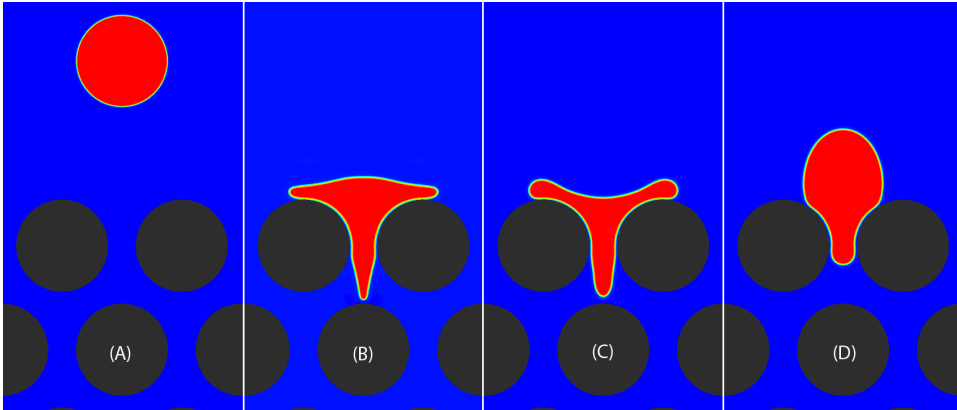


Figure 3: Impact droplet on a paper-like structure with the wetting contact angle $\theta = 180^\circ$. At time reference $t = 0 \mu s$ (A), $17 \mu s$ (B), $34 \mu s$ (C) and $t = 85 \mu s$ (D).

Fig.(2, 3) shows two events as the ink droplet impacts the paper-like structure. The cellulose fibers are mimicked in the simulation by a set of solid circular rods. A non-evaporating droplet with a diameter of $R = 27 \mu m$ impacts onto the two surfaces and it has an initial speed, $u_0 = 6 m \cdot s^{-1}$. The droplet has a density $\rho = 880 kg m^{-3}$, viscosity $\mu = 0.01 Ns m^{-2}$ and surface tension coefficient $\sigma = 0.032 N m^{-1}$. Those physical parameters are relevant to a critical case of dispensing small droplets through a thin liquid film, Do-Quang, Geyl, Stemme, van der Wijngaart, and Amberg (2010). In this study the impact velocity was varied between $u = 4$ and $11 m \cdot s^{-1}$ by varying the dispensing power of the printhead.

Fig.(2) shows the temporal evolution of the droplet shape as it impacts a surface of cellulose fibers with an equilibrium contact angle $\theta = 30^\circ$. As the droplet interacts with the fibers a thin air layer separates the solid surface and the droplet interface. The air layer diffuses into the droplet, and the interface wets the solid, see Fig.(2b). A liquid jet propagates into the paper structure, which finally touches the second layer of fibers (Fig.(2c)). Immediately, the interface forms a contact line with a large apparent contact angle, and the liquid spreads across the fiber. The liquid that penetrates through the two fibers continues to spread onto the papers top fiber layer. This along with the spreading on the second layer, as the droplet relaxes toward its equilibrium shape, squeezes the liquid through the film formed in between the two layers (fig.(2c)) resulting in a film breakup Fig.(2d). A small secondary drop is deposited on the fiber in the second layer and the rest of the droplet forms a footprint on the top layer covering the gap formed between the two horizontally adjacent fibers, see Fig.(2d).

By changing the surface chemistry of the fibers they might become less wettable, resulting in a very different droplet characteristics. Fig.(3) shows the droplet shape at four snapshots in time, as it impacts a paper consisting of fibers with an equilibrium contact angle $\theta = 180^\circ$. First the droplet takes a similar shape in the structure, as observed on a more wettable surface Fig.(2b). However, the air layer separating the solid the interface is retained as it is favored by the surface. As a consequence, the liquid will not wet the second layer in the structure and surface tension contracts the liquid film into a energy minimizing shape, see Fig.(3c). On the top layer the droplet spreads in a similar fashion as observed on a flat surface, where a liquid rim is formed. A second phase in the impact dynamics takes then place as the droplet has decelerated on the surface, as its initial inertial energy is converted into surface energy. The capillary force then contracts the droplet into its energy minimizing shape, so that the droplet bounces back leaving no ink on the paper surface, see Fig(3d).

Fig.(4) shows a snapshots of the droplet shapes of a liquid ink impact into three different paper substrate at $t = 90\mu s$. At that moment, the maximum velocity of the droplet is much smaller than its initial velocity. The initial speed and radius of this droplet and its physical parameters are same as 2D case above. In this figure, we observed the volume of liquid ink that penetrates into the porous medium depend on its chemical energy. For the hydrophilic fibers, case (A) and (B) the liquid ink wets the solid fibers and penetrates into the medium. But in case (C) the liquid ink tends to bounce off the surface as similar in 2D case.

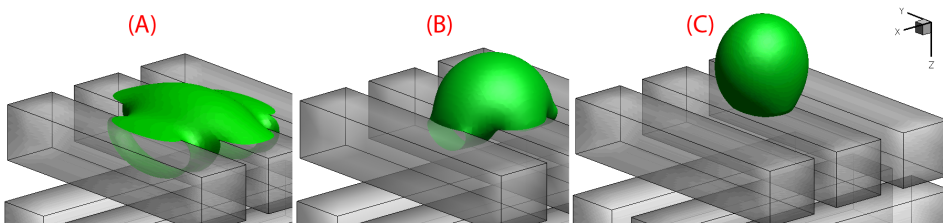


Figure 4: Numerical simulation of a droplet impact and spreading on the different wettable porous medium: (A) the wetting contact angle $\theta = 10^\circ$; (B) $\theta = 90^\circ$ and (C) $\theta = 150^\circ$.

4 Conclusions

In the present paper we have presented two and three -dimensional simulations of ink droplets impacting on a paper-like surface. By only changing the wettability of the cellulose fibers droplets were either deposited on the paper or could bounce off.

This identifies the wettability to be key parameter in order to obtain high quality prints.

The droplet spreading on a highly wettable surface ($\theta = 30^\circ$) shows that secondary droplets can be deposited on the second fiber layer. The droplet was found to significantly decelerate as it penetrated the web of fibers, in compare with the results on a hydrophobic surface ($\theta = 180^\circ$). This points out that energy is stored at the contact line, indicating that the presence of contact lines could even influence macroscopic parameters like the friction coefficient in porous media.

The three-dimensional simulations shows a similar behaviors as two-dimensional simulations. Even though, the impact position of the droplet relative to the upper layer of the rods has been changed.

Acknowledgements

Computer time provided by SNIC (Swedish National Infrastructure for computing) is gratefully acknowledged.

References

- Alam, P.; Toivakka, M.; Backfolk, K.; Sirvio, P.** (2007): Impact spreading and absorption of newtonian droplets on topographically irregular porous materials. *CHEMICAL ENGINEERING SCIENCE*, vol. 62, pp. 3142–3158.
- Amberg, G.; Tönhardt, R.; Winkler, C.** (1999): Finite element simulations using symbolic computing. *Mathematics and Computers in Simulation*, vol. 49, no. 4-5, pp. 257–274.
- Anderson, D.; McFadden, G.; Wheeler, A.** (1998): Diffuse-interface methods in fluid mechanics. *Annual Review of Fluid Mechanics*, vol. 30, pp. 139–165.
- Blake, T. D.** (2006): The physics of moving wetting lines. *Journal of Colloid and Interface Science*, vol. 299, no. 1, pp. 1–13.
- Bonn, D.; Eggers, J.; Indekeu, J.; Meunier, J.; Rolley, E.** (2009): Wetting and spreading. *Rev. Mod. Phys.*, vol. 81, no. 2, pp. 739.
- Cahn, J. W.; Hilliard, J. E.** (1958): Free energy of a nonuniform system. i. interfacial free energy. *The Journal of Chemical Physics*, vol. 28, no. 2, pp. 258–267.
- Carlson, A.; Do-Quang, M.; Amberg, G.** (2009): Modeling of dynamic wetting far from equilibrium. *Physics of Fluids*, vol. 21, no. 12, pp. 121701–4.

- Davis, T. A.** (2004): Algorithm 832: Umfpack v4.3 - an unsymmetric-pattern multifrontal method. *ACM TRANSACTIONS ON MATHEMATICAL SOFTWARE*, vol. 30, no. 2, pp. 196–199.
- Do-Quang, M.; Amberg, G.** (2009): The splash of a solid sphere impacting on a liquid surface: Numerical simulation of the influence of wetting. *Physics of Fluids*, vol. 21, no. 2, pp. 022102.
- Do-Quang, M.; Geyl, L.; Stemme, G.; van der Wijngaart, W.; Amberg, G.** (2010): Fluid dynamic behavior of dispensing small droplets through a thin liquid film. *Microfluidics and Nanofluidics*, vol. 9, pp. 303.
- Do-Quang, M.; Villanueva, W.; Singer-Loginova, I.; Amberg, G.** (2007): Parallel adaptive computation of some time-dependent materials-related microstructural problems. *Bulletin of the Polish Academy of Sciences-Technical Sciences*, vol. 55, no. 2, pp. 229–237.
- Fyfe, D. E.; Oran, E. S.; Fritts, M. J.** (1988): Surface tension and viscosity with lagrangian hydrodynamics on a triangular mesh. *Journal of Computational Physics*, vol. 76, no. 2, pp. 349–384.
- Guermond, J.; Quartapelle, L.** (2000): A projection fem for variable density incompressible flows. *Journal of Computational Physics*, vol. 165, no. 1, pp. 167–188.
- Hyvaluoma, J.; Raiskinmaki, P.; Jasberg, A.; Koponen, A.; Kataja, M.; Timonen, J.** (2006): Simulation of liquid penetration in paper. *Phys. Rev. E*, vol. 73, no. 3, pp. 036705.
- Jacqmin, D.** (1999): Calculation of two-phase navier-stokes flows using phase-field modeling. *Journal of Computational Physics*, vol. 155, no. 1, pp. 96–127.
- Kannangara, D.; Zhang, H.; Shen, W.** (2006): Liquid-paper interactions during liquid drop impact and recoil on paper surfaces. *Colloids and Surfaces A-Physicochemical and Engineering Aspects*, vol. 280, no. 1-3, pp. 203–215.
- Modaressi, H.; Garnier, G.** (2002): Mechanism of wetting and absorption of water droplets on sized paper: Effects of chemical and physical heterogeneity. *Langmuir*, vol. 18, no. 3, pp. 642–649.
- Reis, N.; Griffiths, R.; Santos, J.** (2004): Numerical simulation of the impact of liquid droplets on porous surfaces. *Journal of Computational Physics*, vol. 198, no. 2, pp. 747–770.
- Villanueva, W.; Amberg, G.** (2006): Some generic capillary-driven flows. *International Journal of Multiphase Flow*, vol. 32, no. 9, pp. 1072–1086.

Xu, L.; Barcos, L.; Nagel, S. R. (2007): Splashing of liquids: Interplay of surface roughness with surrounding gas. *Physical Review E*, vol. 76, no. 6.

Xu, L.; Zhang, W.; Nagel, S. (2005): Drop splashing on a dry smooth surface. *Physical Review Letters*, vol. 94, no. 18.

Yarin, A. (2006): Drop impact dynamics: Splashing, spreading, receding, bouncing... *Annual Review of Fluid Mechanics*, vol. 38, pp. 159–192.